Upper Oceanic Energy Response to Tropical Cyclone Passage

JOHN A. KNAFF AND MARK DEMARIA

NOAA/NESDIS–Regional and Mesoscale Meteorology Branch, Fort Collins, Colorado

CHARLES R. SAMPSON, JAMES E. PEAK, AND JAMES CUMMINGS

Naval Research Laboratory, Monterey, California

WAYNE H. SCHUBERT

Department of Atmospheric Science, Colorado State University, Fort Collins, Colorado

(Manuscript received 10 January 2012, in final form 18 October 2012)

ABSTRACT

The upper oceanic temporal response to tropical cyclone (TC) passage is investigated using a 6-yr daily record of data-driven analyses of two measures of upper ocean energy content based on the U.S. Navy's Coupled Ocean Data Assimilation System and TC best-track records. Composite analyses of these data at points along the TC track are used to investigate the type, magnitude, and persistence of upper ocean response to TC passage, and to infer relationships between routinely available TC information and the upper ocean response. Upper oceanic energy decreases in these metrics are shown to persist for at least 30 days—long enough to possibly affect future TCs. Results also indicate that TC kinetic energy (KE) should be considered when assessing TC impacts on the upper ocean, and that existing TC best-track structure information, which is used here to estimate KE, is sufficient for such endeavors. Analyses also lead to recommendations concerning metrics of upper ocean energy. Finally, parameterizations for the lagged, along-track, upper ocean response to TC passage are developed. These show that the sea surface temperature (SST) is best related to the KE and the latitude whereas the upper ocean energy is a function of KE, initial upper ocean energy conditions, and translation speed. These parameterizations imply that the 10-day lagged SST cooling is approximately 0.7°C for a ''typical'' TC at 30° latitude, whereas the same storm results in 10-day (30-day) lagged decreases of upper oceanic energy by about 12 (7) kJ cm^{-2} and a 0.5°C (0.3°C) cooling of the top 100 m of ocean.

1. Introduction

It has been long recognized that the primary energy source for tropical cyclones (TCs) is the ocean (e.g., Palmén 1948; Riehl 1950). Latent and sensible heat is readily drawn from the ocean over the warm tropical and subtropical waters. These energy fluxes are functions of air–sea temperature differences, wind speeds, and relative humidity. As a TC's wind field increases in size and magnitude, the TC extracts an increased amount of energy from the ocean. To continue its intensification, a TC requires a sufficient reservoir of energy. If adequate energy is not available in the ocean (i.e., when the ocean interface is cooler than the surface air in the TC) intensification is halted, except in cases when significant energy is being drawn from the atmospheric environment (i.e., during tropical to extratropical transition).

The scenario above led to the development of the TC potential intensity (PI) thesis, an important concept where the potential TC intensity is determined primarily by the sea surface temperature (SST). Empirical relationships have been developed that describe TC potential intensity as a function of SSTs for various TC basins (Merrill 1987; DeMaria and Kaplan 1994; Whitney and Hobgood 1997; Knaff et al. 2005; Knaff and Sampson 2009). Many empirical and theoretical models of potential intensity have also been developed (e.g., Miller 1958; Emanuel 1986, 1991; Holland 1997, and other references contained therein), which further highlight the importance of the ocean as the primary TC energy source. As the potential intensity concept developed,

Corresponding author address: John Knaff, NOAA/NESDIS/RAMMB, Colorado State University, Campus Delivery 1375, Fort Collins, CO 80523-1375.
E-mail: john.knaff@noaa.gov

DOI: 10.1175/JCLI-D-12-00038.1

potential intensity models incorporated contributions from the overlying atmospheric thermodynamics (e.g., outflow temperature) on the potential intensity. However, under most circumstances, the ocean contribution to potential intensity is greater than or comparable to that of the atmosphere. For this reason we concentrate on changes in the upper ocean for the remainder of this study.

SSTs typically drop with TC passage, being cooled by fluxes of latent and sensible heat, ocean mixing resulting from wind stresses, and wind-driven upwelling (Price 1981, 2009; Black 1983; Shay et al. 1992, 1998; Jacob et al. 2000). This SST cooling reduces the ocean heat flux into the TC and thus limits further intensification (Cione and Uhlhorn 2003; Black et al. 2007; Lin et al. 2008, and references therein). However, it is the turbulent vertical mixing in the upper ocean that is the primary mechanism for cooling the ocean below a TC (Price 1981, 2009; Jacob et al. 2000; Sanford et al. 2007; D'Asaro et al. 2007; Jansen et al. 2010; Dare and McBride 2011)—such mixing is irreversible and while it acts to cool the upper ocean, it also warms the deep ocean, so it should be of interest to the climate community. In fact, the vertical mixing is typically 10 times more effective at cooling the upper ocean than the wind-driven fluxes (Jacob et al. 2000; Cione and Uhlhorn 2003). The effectiveness of the mixing is a function of both the atmospheric forcing and the stratification of the upper ocean, which varies across the regions where TCs typically develop and intensify. The cooling of the ocean surface under a TC is therefore an extremely complicated function of the wind-driven forcing, energy flux out of the ocean, the vertical mixing, and the conditions in the upper portions of the ocean. The recovery of the ocean is also a function of currents, solar insolation, and the upper ocean stratification.

The importance of the upper ocean energy content to TCs, particularly their intensification, has been known for several decades (e.g., Perlroth 1967; Price 1981; Gray 1979; Holliday and Thompson 1979; Shay et al. 2000), but only recently, with the advent of satellite altimeters (circa 1993), has it become possible to study more than a few cases. A quantification of upper oceanic heat content for TC development was first presented by Leipper and Volgenau (1972) as the integrated temperature in excess of 26°C (a commonly used lower limit for TC development) from the depth of the 26°C isotherm ($Z_{26°C}$) to the surface (0), which we will refer to as oceanic heat content (OHC)[1] as defined by

$$\mathrm{OHC}(x,y) = \rho_o C_p \int_{Z_{26°C}}^{0} [T(x,y,z) - 26]\, dz, \quad (1)$$

where $\rho_0 = 1025$ kg m^{-3} and $C_p = 4025$ J kg^{-1} are the mean density and heat capacity of seawater, respectively. Shay et al. (2000) demonstrated the importance of regions of elevated OHC in the intensity evolution of Hurricane Opal (1995)—work that has since led to significant understanding and operational TC intensity forecast capabilities and improvements. OHC has also since been used in a variety of TC research and operational applications as reviewed in Goni et al. (2009). However, Price (2009) pointed out that OHC has shortcomings (OHC is limited to regions of SST $\geq$ 26°C, can misrepresent oceanic conditions in shallow waters, and does not address static stability changes with depth in salt-stratified waters). Price (2009) also proposed that a more relevant measure of upper oceanic energy may be obtained from an average upper ocean temperature as defined by

$$\overline{T_d}(x,y) = \frac{1}{d} \int_{-d}^{0} T(x,y,z)\, dz, \quad (2)$$

where d is the depth of vertical mixing caused by a TC. Price (2009) further described two ways to define the mixing depth d in Eq. (2). The first assumes that the typical mixing depth associated with TC passage is 100 m (a simple yet realistic assumption), and the second calculates the mixing depth directly from the ocean sounding.

The SST cooling associated with TC passage can persist for several weeks and can affect the atmospheric general circulation. Hart et al. (2007) introduced the concept of combined atmospheric and ocean "local memory" due to TC passage via calculation of potential intensities [i.e., PI as described in Emanuel (1986)]. Hart et al. (2007) found that SST cooling resulting from TC passage lasts approximately 40 days where the magnitude of the cooling is a function of TC intensity, but that the atmosphere recovers in about 10 days. Their calculation of maximum potential intensity (MPI), however, showed that the combined oceanic–atmospheric memory lasted longer than 30 days. In a recent and independent study, Dare and McBride (2011) performed a detailed and comprehensive study of SST reduction and recovery time associated with TC passage. They found that in 88% of TC cases the along-track SSTs recovered to climatological values within 30 days and that both TC intensity and translation speed affect SST response and recovery times.

In this study, we will revisit the Hart et al. (2007) and Dare and McBride (2011) SST results, and go further by examining the upper ocean energy changes that also

[1] Leipper and Volgenau (1972) called this quantity "hurricane heat potential." This quantity has also been referred to as "tropical cyclone heat potential" (see Goni et al. 2009, and references contained therein).

occur. We will also attempt to answer a number of questions related to the air–sea energy exchanges with TCs by using a 6-yr daily record of various measures of upper ocean energy content and the TC best tracks during those years. The datasets and their limitations are described in detail in section 2. Given these datasets and their known limitations, we seek to answer the following specific questions with composite analyses:

1) What are the expected cooling and related decrease of energy in the upper ocean after tropical cyclone passage and what are the most important routinely available and observable factors related to the cooling and energy decrease?
2) How long do upper ocean temperature and energy content changes typically persist?
3) Are there any detectable differences between the ocean responses to TCs occurring in different basins (possibly indicating upper ocean stratification differences)?

Note that our study will not address questions related to ocean energy transports or what portion of the upper ocean energy changes result in warming the deep ocean versus warming the atmosphere (i.e., energy partitioning), nor will it discuss detailed results as a function of ocean properties as is done in Shay and Uhlhorn (2008) and Uhlhorn and Shay (2012). Methods used to address these questions are discussed in section 3 and the results are presented in section 4. A summary and discussion is presented in section 5.

2. Data description

A 6-yr period (2005–10) of a real-time 1/6° resolution (~18 km) daily ocean analyses was constructed in a continuous longitudinal domain bounded by 65° north and south latitude. These fields are remapped to a Mercator projection with 1/4° resolution for our analyses. The analyses were obtained using the U.S. Navy Coupled Ocean Data Assimilation (NCODA) system (Cummings 2005). NCODA is a fully three-dimensional, multivariate, optimum-interpolation ocean data assimilation system that produces simultaneous analyses of temperature, salinity, geopotential and u, v vector velocity components. In constructing the ocean analyses, NCODA uses its previous oceanic analysis rather than a model forecast as a first guess in a multivariate optimal interpolation (MVOI) scheme, which makes use of flow-dependent background-error correlations and background-error variances that vary in space and evolve from one analysis cycle to the next. An important feature of NCODA is that an ocean data quality-control system (Cummings 2011) is fully integrated with the MVOI.

The oceanic data for the NCODA analyses are received and processed in real time at the Fleet Numerical Meteorology and Oceanography Center. Most of the data assimilated are made available on the Global Ocean Data Assimilation Experiment (GODAE) data server hosted by the Naval Research Laboratory (http://www.usgodae.org). NCODA assimilates satellite altimeter sea surface height observations,[2] satellite and in situ SST, and in situ vertical temperature and salinity profiles from expendable bathythermographs, Argo floats, and moored buoys, as well as other sources. It is noteworthy that atmospheric wind stresses are not included in the ocean data assimilation, other than through the influence of the winds on the observations, and thus do not directly influence the result. These ocean analyses are a result of a data fitting approach via the NCODA's MVOI and are not influenced or contaminated by model errors, especially those associated with physical parameterization of mixing. The temporal response of the NCODA analysis to new generally sparse and relatively infrequent ocean data at depth, when compared to atmospheric observations, typically takes a few days, which is a common problem in analyses driven solely by oceanic data (e.g., Black 1983; Jansen et al. 2010). Since development of the Argo float array, ~3000 real temperature profiles are assimilated each day in addition to ~3000 synthetic temperature profiles generated from the along-track altimeter sea surface height data using the Modular Ocean Data Assimilation System (MODAS) methodology. Verification of the NCODA analysis relative to the previous analysis (persistence forecast) and analyzed state (residuals) for a 135-day period in 2005 is shown in Cummings (2005; see Fig. 7 therein). In general, persistence forecast temperature errors are higher in western boundary regions such as the Gulf Stream, Kuroshio, Agulhas Current, and Antarctic Circumpolar Current. When averaged as a function of depth persistence, forecast temperature errors are on the order of 0.3°–1.0°C, with maximum errors occurring in the 100–300-m depth range and minimum errors near the surface where the analysis is well constrained by the large amount of satellite SST data assimilated. The analysis procedure reduces these persistence forecast errors considerably to globally averaged values less than ~0.2°C everywhere in the water column. Note that it is the analysis temperature field that is used in this study, so residual errors are the

[2] Sea surface heights from satellite-based altimetry are used along with collocated SST to estimate one-dimensional (vertical) ocean profiles using MODAS (Fox et al. 2002). MODAS profiles are then assimilated in a similar way to real profiles, but with unique error characteristics that reflect the variable skill of the MODAS method and statistical databases across the globe.

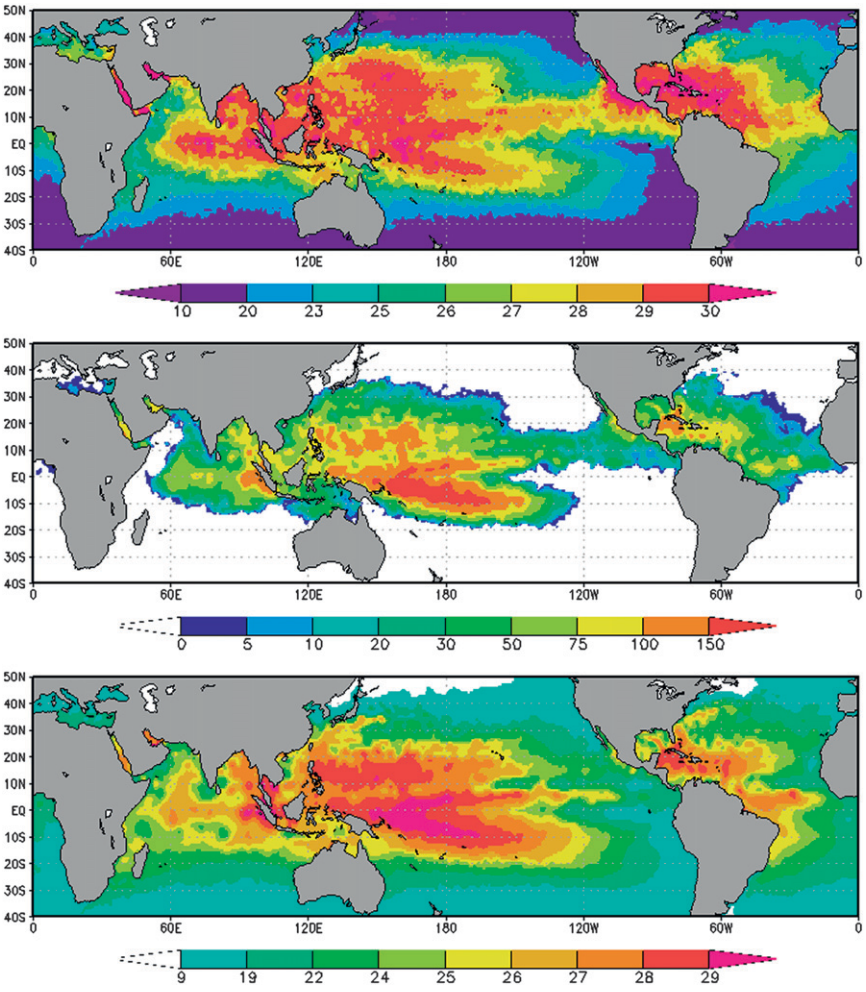

FIG. 1. Examples of daily analysis of (top) SST, (middle) OHC26C, and (bottom) T100M valid on 15 Sep 2005. Units: °C for SST and T100M and kJ cm^{-2} for OHC26C.

proper way to characterize the uncertainty of NCODA. Given this discussion of NCODA capabilities and errors, we believe the global NCODA-based analyses and derived heat content fields are appropriate for the current study.

The NCODA ocean analyses are used to calculate various measures of upper oceanic energy content. These include OHC using Eq. (1), referred to as OHC26C, and the average temperature in the upper 100 m (T100M), which is calculated using Eq. (2). To calculate T100M the variable d in (2) is a fixed value of 100 m or the ocean's bottom if it is shallower, following Price (2009). Other metrics of upper ocean energy content derived from NCODA-based analyses are detailed in Peak et al. (2012, manuscript submitted to *J. Oper. Oceanogr.*) but were not used in this study. Figure 1 shows examples of the SST, OHC26C, and T100M fields valid 15 September 2005.

Monthly climatologies of the upper ocean energy metrics were also constructed using six years of daily analyses. These climatologies are used to estimate/account for the annual variations of the ocean parameters studied here. Because we only had six years of data, 16 passes of a nine-point, spatial, Gaussian filter were applied to the monthly averages constructed from the daily oceanic data files. This filter damps spatial features with horizontal scales less than 150 km, many of which are introduced by averaging just six years of data. The climatology on a given date is estimated by linearly interpolating between the filtered monthly averages, where the monthly climatologies were valid at the median day of that month. Figure 2 shows the 6-yr climatologies matching the dates/times of the SST, OHC26C, and T100M fields in Fig. 1.

TC information used in this study comes from the databases of the Automated Tropical Cyclone Forecast System (ATCF; Sampson and Schrader 2000). Tropical cyclone location, intensity, and operationally important

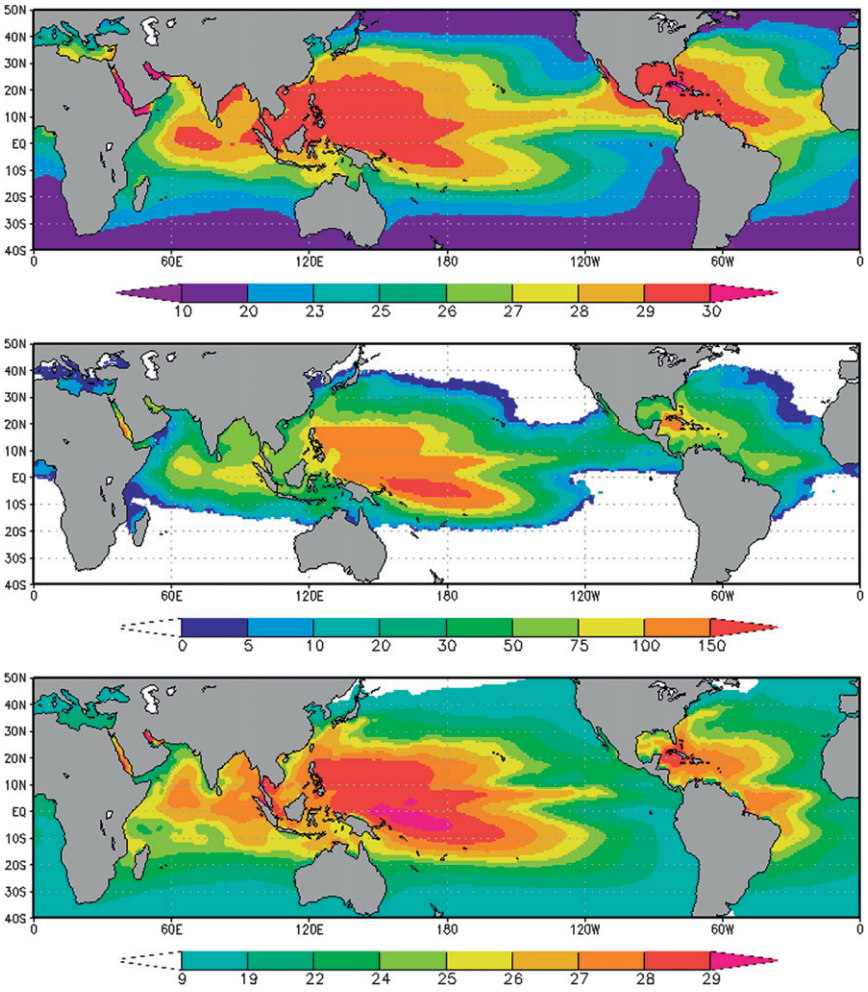

FIG. 2. Examples of 6-yr climatological analyses of (top) SST, (middle) OHC26C, and (bottom) T100M valid on 15 September. Units: °C for SST and T100M and kJ cm^{-2} for OHC26C. Color scaling is the same as in Fig. 1.

wind radii[3] information comes from the best-track archives (or b-decks). The Joint Typhoon Warning Center (JTWC) maintains best-track datasets for TCs occurring in the western North Pacific and Southern Hemisphere. The National Hurricane Center (NHC), which is the World Meteorological Organization's Regional Specialized Meteorological Centre (RSMC), maintains best tracks for the eastern North Pacific and North Atlantic TC basin. The Central Pacific Hurricane Center, also an RSMC, maintains eastern North Pacific records from the date line to 140°W. The best tracks are prepared by the appropriate agency and represent the best poststorm analysis available at the end of each tropical cyclone season but, like any subjectively generated record, they have systematic and random errors due to the way they were constructed, as noted by Landsea et al. (2006). This study makes use of the intensity, positions, and operationally important wind radii contained in the best-track files at 6-hourly intervals; because intensity is reported in knots (kt; 1 kt = 0.514 m s^{-1}), both intensity and translation speed will use this unit for speed throughout this study.

3. Methods

To study the typical ocean response to a tropical cyclone a compositing technique is used. For each 6-hourly, over-ocean (>25 km from shore) TC track position, the ocean variables described in section 2 are interpolated to TC position at eight separate times, including the

[3] Best estimates of the maximum radial extent of 34-, 50-, and 64-kt winds in quadrants around the TC. These have been reanalyzed postseason (i.e., best tracked) beginning in 2004 (Knaff et al. 2007).

concurrent time. Lead/lag times used in this study were 5 days before storm passage, the time of storm passage, and 5, 10, 20, 30, 60, and 90 days following storm passage. Lead and lag times were purposely chosen with a minimum of 5-day intervals to account for the aforementioned typical response time of the analysis to the data. It is recognized that maximum cooling associated with TC passage (e.g., Landis and Leipper 1968) is right (left) of track in the Northern (Southern) Hemisphere, and that poleward moving storms generate westward propagating eddies (Jansen et al. 2010); however, we use the interpolated point values associated with the 6-hourly best-track positions for simplicity. The authors feel that composite averages and/or medians of single point values provide representative estimates of the ocean response and that using area averaged values would likely not improve composite results. This approach is also used independently by Dare and McBride (2011), who provide additional justifications for this approach. This point assumption also allows for a greater number of cases, noting that Jansen et al. (2010) used $15° \times 15°$ areas that would remove cases in key TC formation/occurrence regions such as the Gulf of Mexico, Bay of Bengal, South China Sea, Tasman Sea, Mozambique Channel, Caribbean Sea, and the eastern North Pacific.

The compositing approach discussed above is applied to both the daily ocean variables and the filtered 6-yr climatologies. Since we are interested in the temporal changes of ocean variables prior to and following TC passage, we have to account for similar changes related to the annual cycle. To remove the annual signal, the 6-yr filtered climatological values, interpolated to the track points and times, are first subtracted from the unfiltered daily observations also interpolated to the track point at each lag time to form observation anomaly realizations. The anomaly here refers to the observation minus the climatological value at that point and time. Then the difference between the observation anomaly realizations, one at $t = 0$ and the other at a different time (e.g., 10 days in the future), is calculated to form lagged anomaly differences. Thus for each point along a TC track we can calculate the anomaly differences (annually adjusted changes) in the ocean at a lead time of 5 days and lag times of 5, 10, 20, 30, 60, and 90 days. Since we want our results to be homogeneous, only cases that contain data for all the lead and lag times are included in our statistics.

Using the resulting homogenous 6-yr dataset of these anomaly differences along over-ocean TC tracks, composites based on 1-min sustained maximum wind speed estimates at 10 m, latitude, storm translation speed, initial ocean conditions, and a simplified estimate of kinetic energy (KE), and grouped by TC formation basin, are then formed at each lead and lag time.

The simplified kinetic energy used here is calculated from the operationally important wind radii and intensity information routinely available in the best-track datasets with some simple assumptions regarding the TC size and the radius of maximum winds. This metric is used as a measure of TC energy, noting that frictional velocity, where available, is better related to oceanic mixing balances (Phillips 1977; Kraus and Turner 1967; Pollard et al. 1973). The radius of maximum winds follows the calculations in Knaff et al. (2007) as shown in Eq. (3):

$$r_{\max} = 0.85C[36.1 - 0.0492v_{\mathrm{srm}} + 0.57(|\varphi| - 25)], \qquad (3)$$

where C is the conversion from nautical miles to kilometers, $v_{\mathrm{srm}} = v_{\max} - 1.5c^{0.63}$ is the storm-relative intensity in knots, and φ is latitude in degrees. A factor of 0.85 is used to account for some of the high bias in $r_{\max}$ estimates (Knaff et al. 2007). The formula $v_{\mathrm{srm}} = v_{\max} - 1.5c^{0.63}$ assumes that the intensity ($v_{\max}$) and translation speed (c) have units of knots following the Schwerdt et al. (1979) asymmetry factor. This implies that rapidly translating TCs will result in slightly larger radii of maximum winds. Average values of the operationally important wind radii from the best track are then calculated, excluding all zeros. For instance, if the four wind radii quadrants are reported as 0, 50, 100, and 0 nautical miles, the nonzero average would be 75 nautical miles. Eliminating the quadrants with zero wind radii from the average removes noise from the data for cases where the maximum wind is close to the 34-, 50-, or 64-kt wind radii threshold (Demuth et al. 2006).

To calculate a simplified kinetic energy, a linear piecewise approach is used to create a wind field using all available wind radii values. The wind speed is assumed to increase from zero at $r = 0$ to V_{srm} at $r = r_{\max}$ (the radius of maximum winds). It then decreases to 64 kt at the nonzero average 64-kt wind radius, and so on to the 34-kt nonzero wind radius. It then decreases to zero at $r = 650$ km. The estimate of 650 km as the radius of zero TC wind is based on rawinsonde composite observations that suggest the typical TC circulation extends 6° latitude from the TC center. This is a region where little or no convection occurs, average vertical motion is close to zero, and the boundary layer vorticity and divergence switch signs (Frank 1977). Fewer linear segments are used if some azimuthally averaged wind radii are zero. The minimum number of linear segments is two (i.e., $r = 0$ to $r = r_{\max}$ and $r = r_{\max}$ to $r = 650$ km). For all the KE computations, the density of air is assumed to be 1 kg m^{-3} and the vertical depth is assumed to be 1 m.

For the remainder of this paper, we will primarily concentrate on the ocean response to TC passage in

TABLE 1. Bin thresholds associated with the composite analysis used in this study and presented in section 5. Units for SST, OHC26C, T100M, storm speed, storm intensity, and storm KE are °C, kJ cm^{-2}, °C, kt, kt, and J ($\times 10^7$), respectively.

Bin threshold	Initial SST	Initial OHC26C	Initial T100M	Storm speed	Storm intensity	Storm KE	Storm latitude
1	25	10	23	4	35	3.0	12.5
2	26	30	24	8	55	6.0	17.5
3	27	50	25	12	77	9.0	22.5
4	28	70	26	16	102	12.0	27.5
5	29	100	27	20	127	16.0	32.5

terms of SST, OHC26C, and T100M that have been composited by five factors, namely, their initial conditions, translation speed, intensity, KE, and latitude. To form composites of these three measures of ocean energy, we employ six bins to parse the observations by these five factors, yielding 30 different composites for SST, OHC26C, and T100M. Table 1 shows the factor thresholds associated with each bin used in our composite analyses. Note that the first bin contains the composites associated with values less than that of bin threshold 1 and that the sixth bin contains composites associated with values greater than or equal to bin threshold 5. We will use means and standard deviations in composites of the continuous SST and T100M, but medians and quartiles in the composites of positive semidefinite OHC26C. These measures of expected value and spread are most appropriate for the composites given nature of the observations and the distributions of the anomalies. Table 2 shows the number of cases available for each bin and compositing variable (see table caption for details), noting that the positive semidefinite nature of OHC26C reduces the number of cases.

4. Results

a. Initial ocean response

We initially present results that concentrate on the time period 10 days following TC passage since some of the datasets used by NCODA, particularly the satellite-based altimetry, have refresh times of approximately five days. Altimetry data are important in assessing the upper ocean's temperature structure including eddies and fronts with warmer regions of the ocean associated with elevated sea surface heights. This 10-day lag time also allows the relatively sparse sounder data to propagate through the analysis via the variational data assimilation (i.e., the MVOI in NCODA) and the TC signal, if present in our composites, should be most obvious.

Figure 3 shows the 10-day response (means with 1 sigma bars) of the SST as a function of initial SST, storm speed, intensity, and KE and further stratified by TC basin. Greater SST cooling appears to be a function of warmer initial SSTs. This is thought to be a result of two factors: the tendency for stronger TCs over warmer waters, and the fact that very warm SSTs (>29°C) are often associated with relatively shallow stable bodies of water that are rapidly mixed and thus cooled by any strong wind. It also appears that slower moving storms generally result in greater SST cooling in most basins [Atlantic (ATL), eastern Pacific (EPAC), and Southern Hemisphere (SHEM)], but there is a lot of interbasin variability (Fig. 3, top right). The relationship in ATL, EPAC, and SHEM is likely due to the occurrence of prolonged upwelling, evaporation, and mixing with the slower moving storms. Greater cooling is anticipated with more intense TCs as the stronger winds would result in greater mixing, with all other factors held constant. In Fig. 3 (bottom left) the intensity-based composites show that the 10-day lagged SST cooling associated with a strong tropical storm is 0.4°C, nearly twice that for a hurricane/typhoon. Another interesting feature is the greater cooling in the Atlantic storms in the 60- to 100-kt range of intensities, which may be an artifact related to the tendency for hurricanes to grow while weakening and moving northward (Merrill 1984; Knaff et al. 2007; Maclay et al. 2008). In the western North Pacific results show that the most cooling is associated with the most intense TCs, which may suggest that the most intense TCs in that basin occur in a region more susceptible to mixing, move slower, or have larger wind fields than in other basins. It appears from the global result that after 10 days tropical storms cool the SSTs about half as much as hurricane-strength TCs, which cool the SSTs on average by about 0.6°C. These results also agree well with the Dare and McBride (2011) day-10 values (~0.35°C) for all TC cases shown in their Fig. 5a.

Figure 3, bottom right, shows the SST changes as a function of TC KE, as defined in section 3. This allows us to account for some of the variations in the size and overall strength of the wind field and how those are related to post-TC SST changes, accepting that the response to a given wind field is also a function of upper ocean static stability. We get the expected result, namely that TCs with larger values of KE result in greater SST cooling. The relationship between KE and SST cooling

TABLE 2. The number of cases contained in each compositing bin as a function of compositing variable. Note there are two columns of numbers for the storm speed, intensity, KE, and latitude composites. The first is valid for SST and T100M composites and the second for OHC26C composites.

Bin	Initial SST	Initial OHC26C	Initial T100M	Storm speed	Storm intensity	Storm KE	Storm latitude
				Atlantic			
1	229	37	408	161, 86	933, 721	1032, 797	159, 159
2	117	307	257	540, 354	629, 383	555, 366	569, 540
3	199	402	296	646, 421	404, 173	255, 121	487, 446
4	421	346	286	479, 360	118, 81	114, 53	356, 238
5	619	294	357	282, 207	96, 84	76, 45	342, 74
6	627	69	609	104, 45	32, 31	180, 91	299, 16
				Eastern North Pacific			
1	260	130	1296	299, 209	1320, 912	1483, 1054	332, 332
2	191	753	444	843, 578	559, 414	654, 483	1274, 1121
3	283	549	353	840, 609	327, 223	178, 106	628, 267
4	530	166	178	379, 276	137, 100	64, 43	158, 7
5	808	53	77	70, 50	65, 50	32, 16	36, 1
6	365	7	89	6, 6	29, 29	26, 26	9, 0
				Western North Pacific			
1	57	21	168	226, 200	1097, 976	1372, 1201	495, 495
2	63	139	111	764, 670	684, 488	677, 484	781, 758
3	103	304	240	918, 753	532, 408	315, 245	877, 766
4	267	451	334	623, 509	322, 242	210, 142	389, 257
5	821	765	441	230, 153	193, 139	150, 103	220, 46
6	1596	622	1613	146, 39	79, 71	183, 149	145, 2
				Southern Hemisphere			
1	146	123	131	433, 398	1364, 1157	1665,1429	694, 672
2	190	602	130	1254, 1112	812, 675	851, 707	1279, 1193
3	428	812	274	818, 694	488, 414	282, 234	781, 644
4	772	551	788	391, 309	229, 202	164, 146	263, 104
5	853	341	970	98, 63	157, 145	73, 69	55, 2
6	683	83	779	78, 39	22, 22	37, 30	0, 0
				Global			
1	692	315	2006	1194, 966	4895, 3944	5782, 4708	1877, 1852
2	561	1863	954	3606, 2916	2834, 2107	2877, 2177	4042, 3748
3	1023	2167	1216	3327, 2581	1807, 1274	1055, 731	2834, 2184
4	2058	1624	1657	1897, 1479	814, 633	556, 388	1184, 624
5	3259	1554	1960	685, 478	526, 433	341, 243	653, 123
6	3450	812	3253	334, 129	167, 158	432, 302	453, 18

appears to be nearly linear through 10^8 J, with the higher values of KE showing large basin-to-basin variability. This result, along with the adjacent intensity composite (which shows less of a correlation), suggests that the size of the wind field is more strongly related to SST cooling than TC intensity alone. For example, the largest and most energetic TCs result in an average 10-day SST cooling of around 1°C—larger than the 0.6° to 0.7°C associated with the most intense storms.

The analyses of SSTs only provide insight into what happens at the ocean surface, so we examined the cooling in the upper ocean with composites of OHC26C and T100M, which are shown in Fig. 4 (medians and quartile range bars) and Fig. 5 (means and 1 sigma bars), respectively. These figures along with Fig. 3 help address several of the questions posed in section 1 about the cooling and energy decrease of the upper ocean during TC passage. In some respects the composite results shown in Figs. 4 and 5 are easier to interpret than those shown in Fig. 3. The results show much clearer relationships between upper ocean energy changes and storm translation speeds (nonlinear), intensity, and KE (linear). There is also a clear signal associated with the initial OHC26C values, suggesting that larger energy decreases are associated with those TCs with larger initial values of OHC26C.

Figure 4 shows 10-day changes in OHC26C. The results are similar to those associated with SSTs. OHC26C changes as a function of initial OHC26C. This relationship may be enhanced by the positive semidefinite nature of OHC26C. Greater energy decreases are associated with slower moving storms, echoing the findings of Lin et al. (2009). The OHC26C changes appear nonlinear with respect to storm translation speeds, suggesting that mixing and upwelling may be more important for nearly

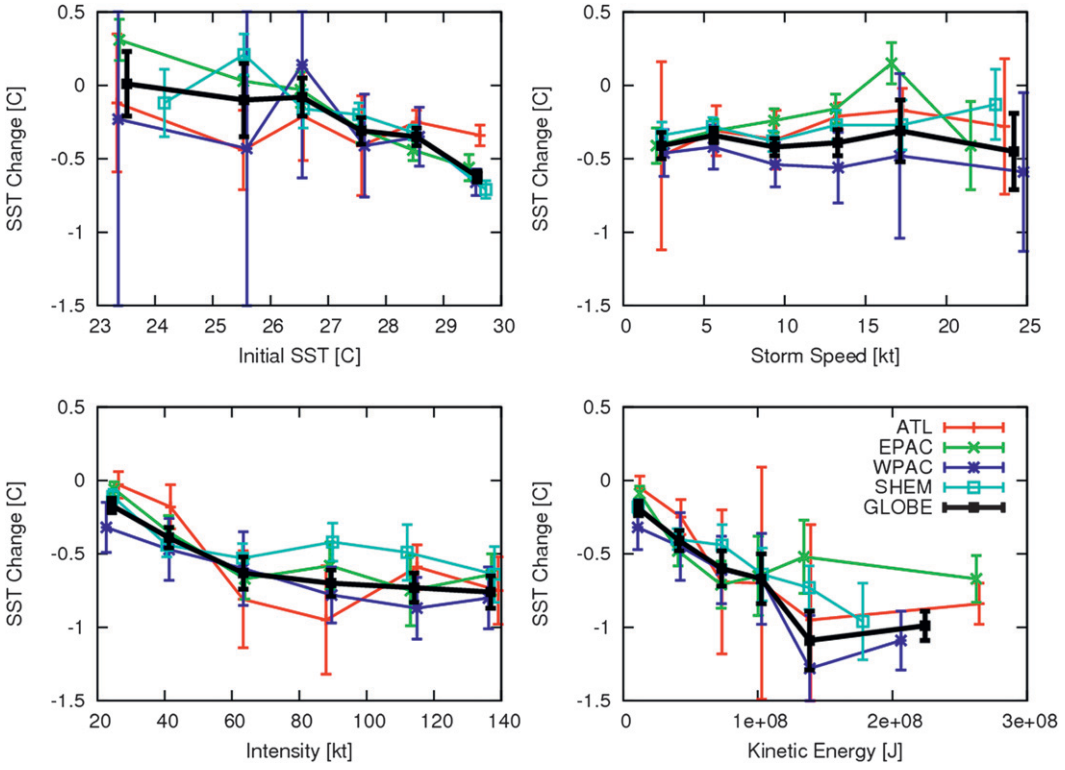

FIG. 3. The 10-day SST response to the passage of a tropical cyclone as a function of (top left) initial SST, (top right) storm speed, (bottom left) intensity, and (bottom right) kinetic energy. Mean values are indicated by the points and the bars indicate the 1 sigma value from the mean. Results are shown for the Atlantic (ATL, red), the east and central Pacific (EPAC, green), the northwest Pacific (WPAC, blue) and Southern Hemisphere (SHEM, magenta) TC basins, as well as the global response (GLOBE, black).

stationary storms. Higher intensity and KE storms also tend to result in greater decreases of energy from the upper ocean—those relationships appear more linear in nature. The composite median results suggest that the 10-day upper ocean energy decrease for a typical global hurricane-strength TC that is moving at typical speeds and has average size is about 0–25 kJ cm^{-2} with a median of approximately 10 kJ cm^{-2}. These results are in line with in situ results obtained by Shay and Uhlhorn (2008).

More interesting are the interbasin differences. It is clear that the typical TC in western North Pacific (e.g., one that has KE of 10^8 J) results in greater decreases in upper ocean energy, nearly twice as much as eastern North Pacific TC cases. This result is evident in all composites of OHC26C. Thus it appears that TCs of equal size and intensity can result in greater decreases in the upper ocean energy in the western North Pacific. It is interesting to note that the energy decreases associated with east Pacific TCs are the smallest and that the energy decreases that occur in the Atlantic and Southern Hemisphere cases are closer to the median/mean values. This difference is likely caused by differences in upper ocean static stability, as discussed in general in Price (2009) and detailed specifically for the eastern North Pacific by Shay and Brewster (2010). This result suggests that more investigation is needed to determine the specific causes of these interbasin differences.

One would initially expect the T100M results (Fig. 5) to be nearly identical to those in Fig. 4, and they are for the global result. Globally and after 10 days the typical hurricane-strength TC will cool the upper ocean on average by about 0.3° to 0.5°C. A ''back of the envelope'' calculation of heat content assuming 100-m depth is that 1°C cooling is approximately 41 kJ cm^{-2}. So these numbers are consistent, but a little larger than the OHC26C composites. However, the interbasin results are quite different. Notable differences include the different OHC26C slopes of the east and west Pacific with respect to intensity and KE, and the relationships to the initial conditions in which T100M composites have larger interbasin variability. Some of the difference is due to plotting means in Fig. 5 versus medians in Fig. 4. The more notable difference is in the east Pacific where there is evidence that interannual variation of the upper ocean (i.e., thermocline depth variations associated with

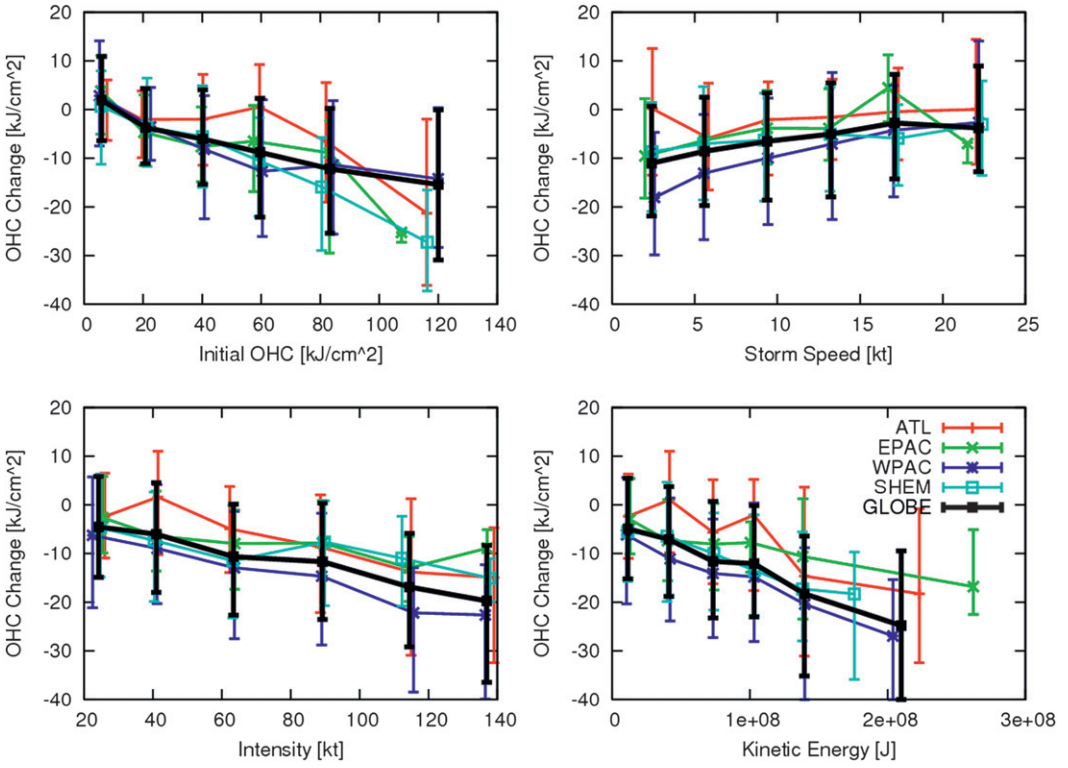

FIG. 4. The 10-day OHC26C response to the passage of a tropical cyclone as a function of (top right) storm speed, (bottom left) intensity, and (bottom right) kinetic energy; initial OHC26C conditions are shown at top left. Median values are indicated by the points and the bars indicate the quartiles of the distribution. Results are shown for the Atlantic (ATL, red), the east and central Pacific (EPAC, green), the northwest Pacific (WPAC, blue) and the Southern Hemisphere (SHEM, magenta) TC basins as well as the global response (GLOBE, black).

El Niño–Southern Oscillation) may result in greater variability in the measurement of T100M—noting here that TC activity in the east Pacific is generally enhanced and the thermocline is also deeper in El Niño conditions.

b. *Persistence of observed changes*

Shifting focus to the length of time that the mean cooling of the ocean lags TC passage, we first examine the persistence of SST cooling. Figure 6 shows SST anomalies for 10, 30, 60, and 90 days following TC passage as a function of KE (note that 20-day lags are not shown for brevity as the results at those lags can be easily inferred from the 10-day and 30-day lags). Here we also find evidence of at least a 30-day recovery time as shown by Hart et al. (2007) and confirmed by Dare and McBride (2011), but because KE accounts for variations of the TC size, intensity, and strength as defined by Merrill (1984), the results here imply that larger and stronger TCs not only result in more initial cooling, but that cooling tends to persist for a longer period of time. Even the lower values of KE show persistent cooling through 60 days, and the cooling for the high KE systems is still on the order of 0.5°C after 60 days. Composites of 90-day persistence also show negative global SST anomalies, but these are much more difficult to interpret as the intrabasin comparison from one time to the next is not always consistent, suggesting other seasonal and longer-term factors become more important at these longer lag times, noting again that the annual cycle has been removed from these calculations.

Figure 7 shows the OHC26C persistence in the same manner as Fig. 6. Here the typical changes in OHC26C, much like the SSTs, were found to persist through roughly 60 days. Again there is an indication that there is a net reduction of energy in the upper ocean and that the greater the KE, the greater the initial decrease in OHC26C and the slower the recovery to near, if not slightly less energetic ocean conditions. It is interesting to note that even at lags of 90 days negative OHC26C changes are still present in global medians, suggesting that TC passage effects continue to linger after the typical TC season. Not all basins (i.e., the eastern North Pacific) show negative anomalies at 90 days and the spread increases noticeably, suggesting that other seasonal and longer-scale phenomena begin to dominate the signal at lags longer than 60 days. Examining the upper ocean temperature

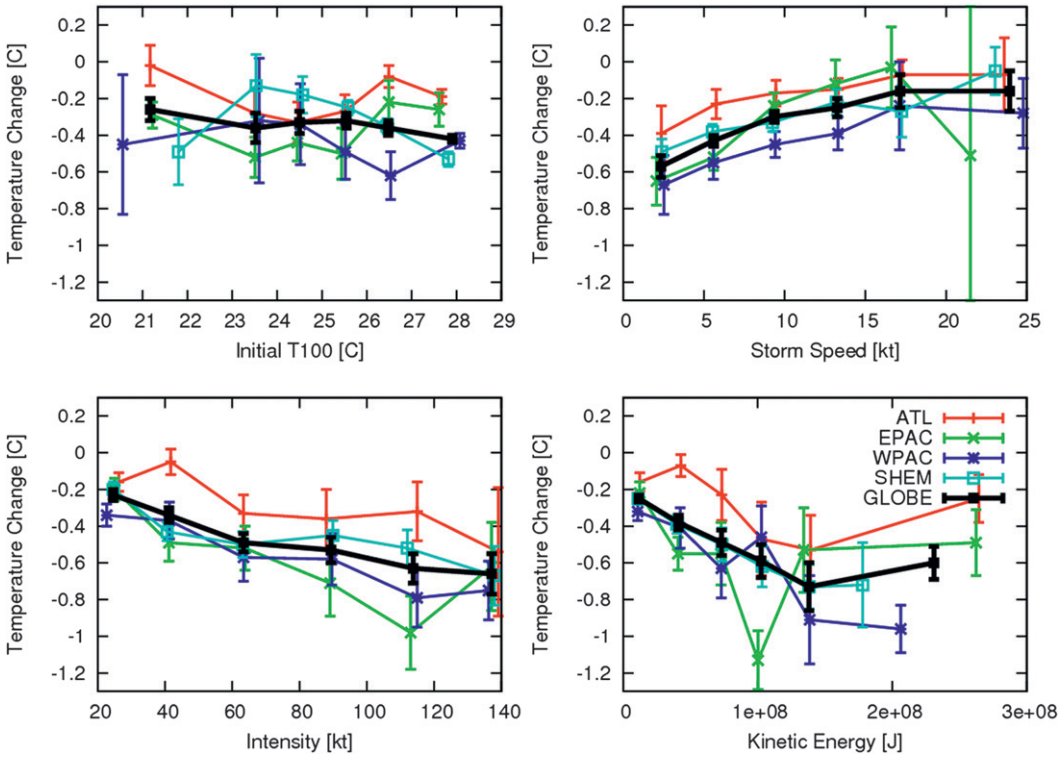

FIG. 5. The 10-day T100M response to the passage of a tropical cyclone as a function of (top right) storm speed, (bottom left) intensity and (bottom right) kinetic energy; initial T100M conditions are shown at top left. Mean values are indicated by the points and the bars indicate the 1 sigma value from the mean. Results are shown for the Atlantic (ATL, red), the east and central Pacific (EPAC, green), the northwest Pacific (WPAC, blue) and Southern Hemisphere (SHEM, magenta) TC basins as well as the global response (GLOBE, black).

changes using T100M offers a different perspective. Figure 8 shows the lag time composite of T100M versus KE. Here the net cooling is evident though 30 days and there is some evidence that this persistence lasts through 60 days; however, the 60-day lagged T100M composite indicates that the Southern Hemisphere and possibly the eastern North Pacific basins have recovered. Our results indicate that T100M may not be appropriate where the thermocline is shallow (less than 100 m) or where its depth varies greatly annually and interannually. These conclusions are similar to those of Shay and Brewster (2010), who showed that the stable stratification of the east Pacific also makes the 100-m mixed layer depth a poor assumption.

c. *Parameterization of changes*

A potentially useful exercise for climate applications is to determine the measurable factors (those examined above plus TC latitude) that are most important to the post-TC ocean responses and derive the lagged mean response based on those factors. Since the factors examined covary to a large degree and we are interested in a stable yet simple result, the composited results (i.e., multiple composites) will be used to develop the simplest and most skillful multiple linear regressions.

Regression equations based on our composite results suggest that lagged SST cooling is best related to two factors from Table 2, namely the KE and the latitude.[4] This regression equation for SST explains roughly 57%, 60%, 45%, and 45% of the variance in the dependent composited data at lags of 5, 10, 20, and 30 days, respectively. The form of the equation is provided in (4) and the coefficients, which are significant at the 95% level, are provided in Table 3.

$$\Delta\mathrm{SST} = A + C_{\mathrm{KE}}\mathrm{KE} + C_{\varphi}|\varphi|. \qquad (4)$$

The linear relationship with latitude (φ) and KE suggests that other factors related to latitude (subsurface

[4] If using storm translation speed instead of latitude, the regression for the 10-day lagged response the variance explained is reduced to 57%. Forcing translation speed into the regression equation that also includes latitude variations increased the variance explained by (4) by just 2%. This remains true for other regression equations.

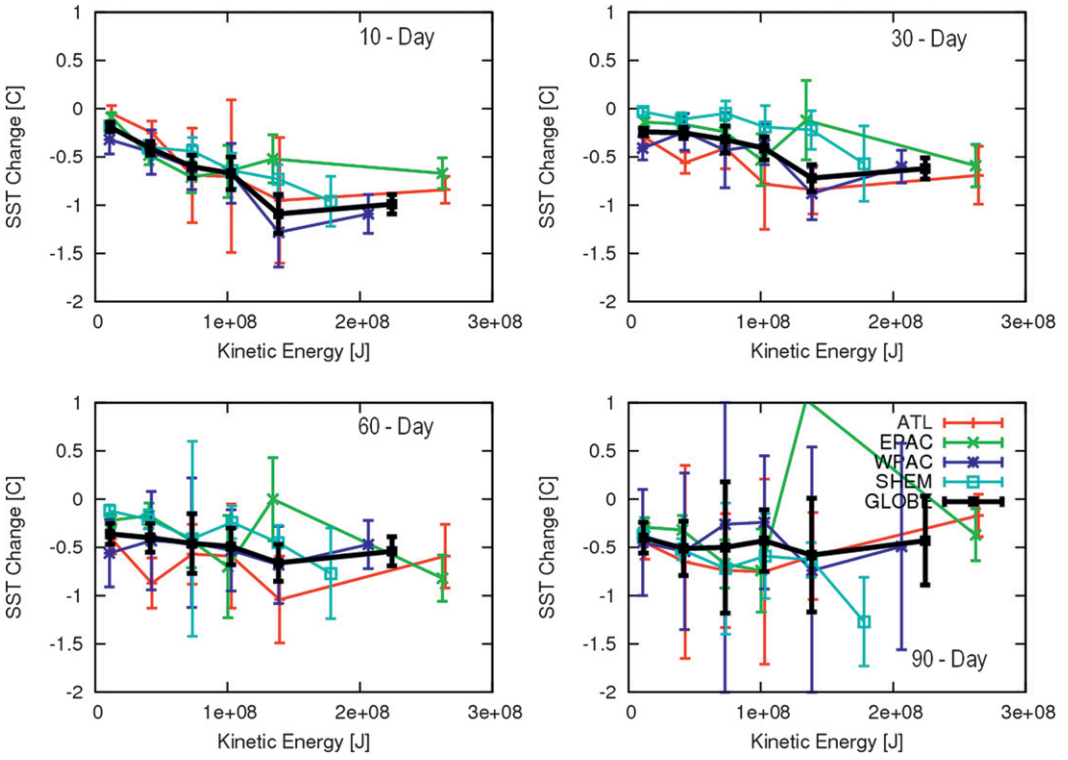

FIG. 6. Mean SST changes as a function of KE at (upper left) 10 days, (upper right) 30 days, (lower left) 60 days, and (lower right) 90 days following TC passage. Mean values are indicated by the points and the bars indicate the 1 sigma value from the mean. Results are shown for the Atlantic (ATL, red), the east and central Pacific (EPAC, green), the northwest Pacific (WPAC, blue) and Southern Hemisphere (SHEM, magenta) TC basins as well as the global response (GLOBE, black).

conditions, translation speeds, and the wind-driven upwelling) are also important for SST cooling. For instance, this implies that a typical TC (KE = 1.0×10^8) at 30° latitude results in a SST cooling of 0.66°, 0.70°, 0.60°, and 0.73°C on average at lags of 5, 10, 20, and 30 days, respectively. Note that the 30-day regression equations are more heavily weighted to the latitude parameter and less to the TC, suggesting that the influence of the TC is weakening and much of the cooling is related to factors related to latitude variations. For this reason we recommend using the 30-day SST cooling parameterization with caution.

On the other hand, the lagged response in OHC26C and T100M appears most related to three factors: translation speed, KE, and initial conditions. The 5-, 10-, 20-, and 30-day lagged regressions on median OHC26C explain 90%, 96%, 88%, and 66% and 79%, 81%, 70%, and 32% of the variance of mean T100M, respectively. The resulting form of the parameterizations for OHC26C and T100M are shown in Eqs. (5) and (6), respectively. The coefficients are provided in Table 3.

$$\Delta\mathrm{OHC26C} = A + C_{\mathrm{spd}}\mathrm{SPD} + C_{\mathrm{KE}}\mathrm{KE} + C_{\mathrm{OHC26C}}\mathrm{OHC26C}_{t=0}, \quad (5)$$

$$\Delta\mathrm{T100M} = A + C_{\mathrm{spd}}\mathrm{SPD} + C_{\mathrm{KE}}\mathrm{KE} + C_{\mathrm{T100M}}\mathrm{T100M}_{t=0}. \quad (6)$$

These equations indicate that a typical TC (KE = 1.0×10^8) moving at 10 kt with initial OHC26C of 50 kJ cm^{-2} and initial T100M of 28°C typically results in OHC26C reductions of 10.5, 11.7, 9.3, and 6.3 kJ cm^{-2} at 5, 10, 20, and 30 days following storm passage, respectively. Similarly, T100M is reduced by 0.47°, 0.53°, 0.41°, and 0.33°C at lags of 5, 10, 20, and 30 days. From the equations above and from results shown in Figs. 5–7 it is apparent that the integrated quantities (OHC26C and T100M) are less variable and thus more predictable than the SST. This suggests that the integrated quantities are possibly more applicable for TC attribution and sensitivity studies.

d. Individual TC examples

Sections 4a and 4b showed (based on composites of large numbers of cases) the average SST, OHC26, and T100M responses (i.e., 10 days after) to TC passage and indicated that those responses persist for 30 days or longer. To get a better sense of the effects in individual

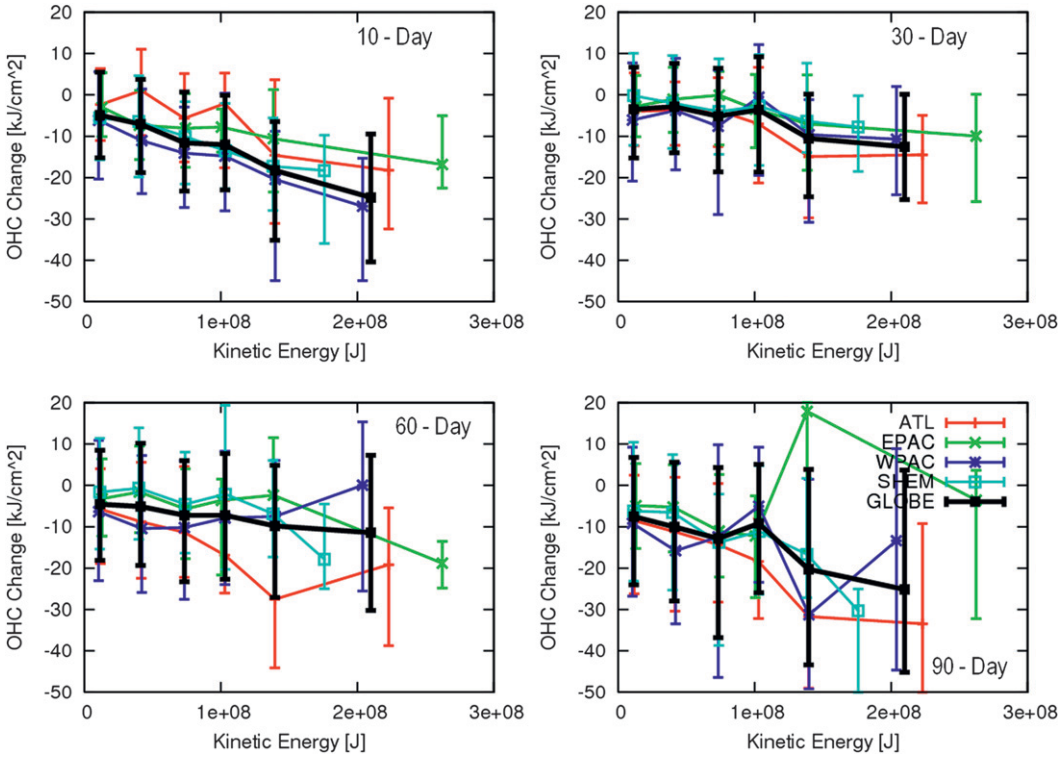

FIG. 7. Typical OHC26C changes as a function of KE at (upper left) 10 days, (upper right) 30 days, (lower left) 60 days, and (lower right) 90 days following TC passage. Median values are indicated by the points and the bars indicate the quartile values from the median. Results are shown for the Atlantic (ATL, red), the east and central Pacific (EPAC, green), the northwest Pacific (WPAC, blue) and Southern Hemisphere (SHEM, magenta) TC basins as well as the global response (GLOBE, black).

cases, three relatively long-lived individual TC cases from 2011 are now examined. Figure 9 shows the best-track locations, dates, and 34-kt wind radii of Typhoon Megi in the western North Pacific (15W), Tropical Cyclone Ului in the Southwest Pacific (20P), and Hurricane Igor in the North Atlantic (11L).

Figures 10, 11, and 12 show time series plots for Typhoon Megi, Tropical Cyclone Ului, and Hurricane Igor, respectively. In each of these figures the temporal evolution of the intensity and KE are shown in the top panel and T100M at 5-day lead and 5-, 10-, 30-, and 60-day lag times are shown in the subsequent panels. Note the dates shown on the panels are associated with the TC location at a lag of zero days and locations can be inferred using the information in Fig. 9.

In the case of Typhoon Megi (Fig. 10), the T100M changes 5 and 10 days following TC passage show a remarkable correspondence with the time series of KE. The maximum along-track cooling at 10 days is on the order of 4°–5°C and is associated with the KE maximum, noting again the possibility of a lagged response due to data availability. Following those times the effects of advection, upwelling, mixing, and solar heating act to relax the along-track changes, but even after 60 days the cooling associated with maximum intensity and to a small degree the maximum KE is still visible.

A similar evolution is seen with Tropical Cyclone Ului (Fig. 11), which shows that the along-track T100M cools approximately 1° to 2°C by 10 days (5-day cooling is most evident in points following 15 March initial times) following TC passage, and that the magnitude of those changes closely corresponds to the time series of KE. Again, as was the case with Megi, other processes erode the residual cooling, which is only barely evident at 30- and 60-day lags.

The upper ocean response to Hurricane Igor is shown in Fig. 12. The T100 response appears to be better correlated to the intensity than the KE, noting that Igor's wind field continues to grow as the storm becomes post tropical (see the large 34-kt wind radii in Fig. 9). The maximum T100M cooling is on the order of 2°–3°C. In contrast to Megi and Ului, the upper oceanic response is generally more persistent. In fact, the resulting TC-induced cooling signature in the tropics remains intact even 60 days after TC passage. It also appears that the changes at higher latitudes do not persist as long as

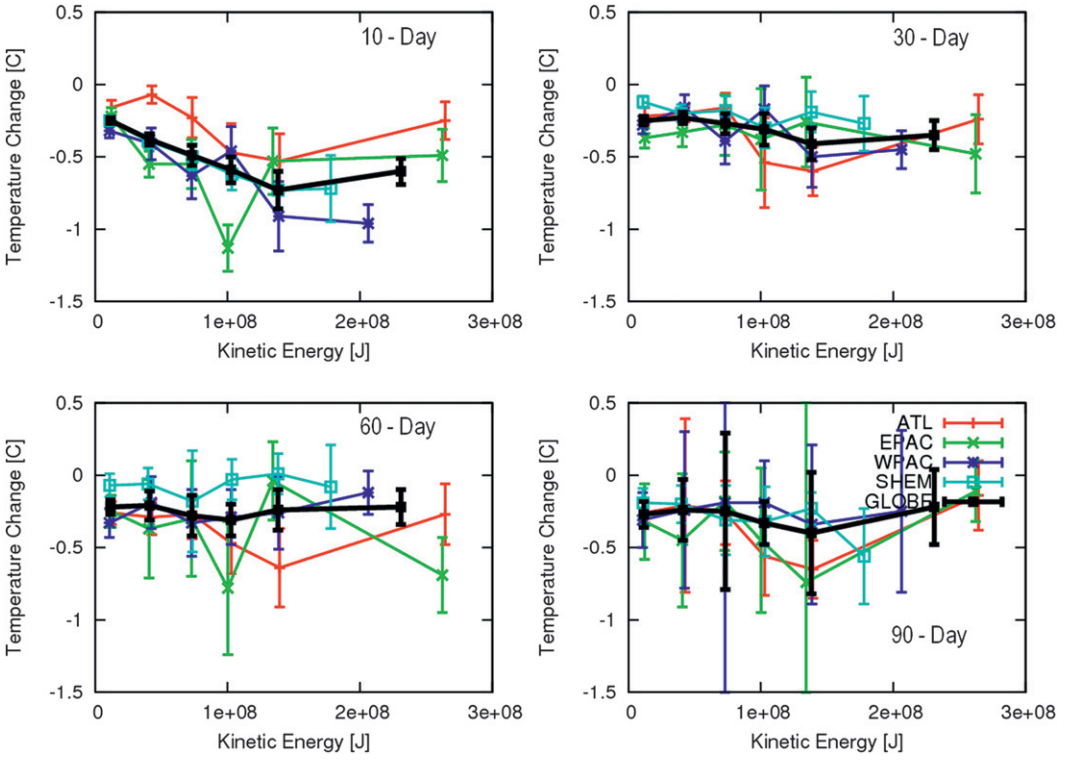

FIG. 8. As in Fig. 6, but for T100M.

changes nearer the equator, which suggests that wind stresses and advection play a larger role in ocean recovery at these latitudes. Stronger wind stresses here are due to the more frequent passage of midlatitude cyclones and the strengthening of westerly winds with the onset of winter. Advection is likely enhanced by propagating eddies away (east and west) generated by the poleward portions of Igor's track (Jansen et al. 2010). Note that

TABLE 3. Variance explained and related regression coefficients for the lagged SST, OHC26C, and T100M changes at 5, 10, 20, and 30 days following TC passage. Regression coefficients met the 95% significance level. Values are valid along the TC track.

			SST		
Lag	R^2	A	C_{KE}	C_{φ}	
5-day	0.57	2.3480×10^{-1}	-4.3517×10^{-9}	-1.5689×10^{-2}	
10-day	0.60	0.2704×10^{-1}	-3.7992×10^{-9}	-1.1310×10^{-2}	
20-day	0.45	2.1047×10^{-1}	-2.6357×10^{-9}	-1.8323×10^{-2}	
30-day	0.45	4.1523×10^{-1}	-1.8819×10^{-9}	-3.1888×10^{-2}	
			OHC26C		
Lag	R^2	A	C_{KE}	C_{spd}	C_{OHC26C}
5-day	0.90	3.0927	-7.4519×10^{-8}	3.7981×10^{-1}	-1.0746×10^{-1}
10-day	0.96	0.4517	-8.3026×10^{-8}	5.0222×10^{-1}	-1.5980×10^{-1}
20-day	0.88	2.7892	-5.1709×10^{-8}	2.0556×10^{-1}	-1.6002×10^{-1}
30-day	0.66	3.0927	-3.3498×10^{-8}	0.9022×10^{-1}	-1.5835×10^{-1}
			T100M		
Lag	R^2	A	C_{KE}	C_{spd}	C_{T100M}
5-day	0.79	0.7496×10^{-1}	-2.1244×10^{-9}	1.2533×10^{-2}	-0.7645×10^{-2}
10-day	0.81	3.2098×10^{-1}	-2.3942×10^{-9}	2.0018×10^{-2}	-0.4836×10^{-2}
20-day	0.70	1.0027×10^{-1}	-1.5443×10^{-9}	1.5008×10^{-2}	-1.8413×10^{-2}
30-day	0.32	-0.4270×10^{-1}	-0.8222×10^{-9}	0.4593×10^{-2}	-0.9003×10^{-2}

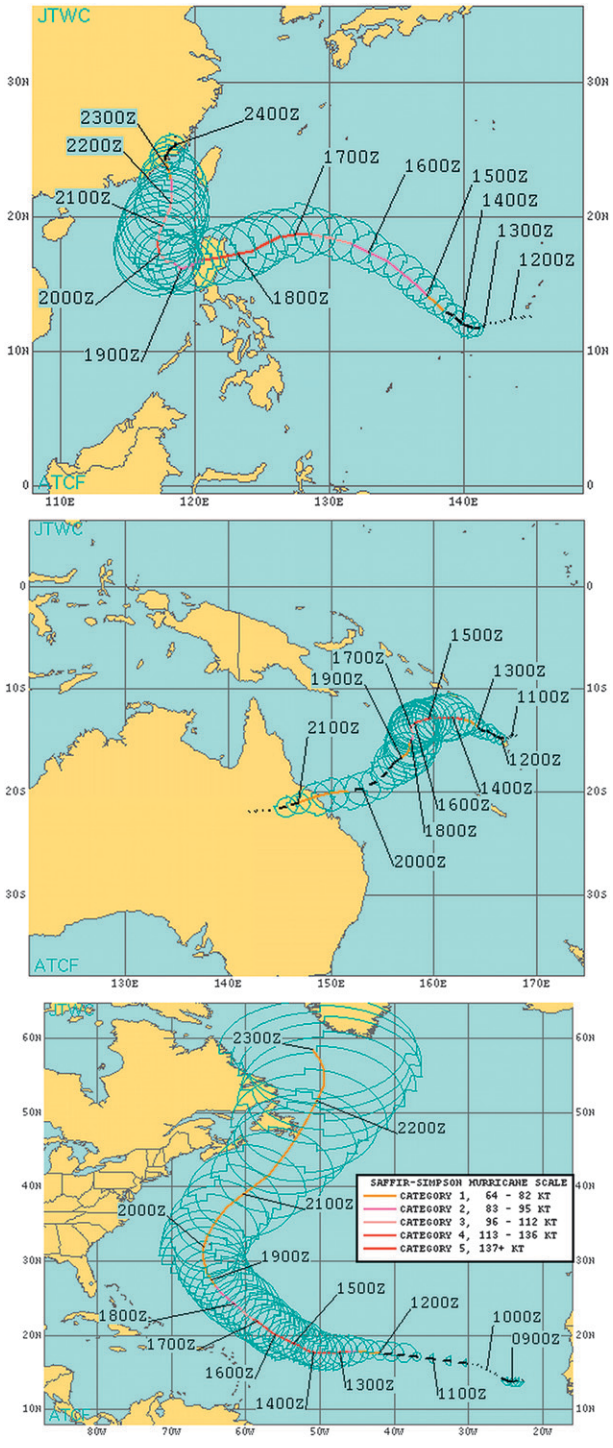

FIG. 9. Best-track locations, dates (day of the month at 0000 UTC) and 34-kt wind radii for Typhoon Megi (15W, western North Pacific), Tropical Cyclone Ului (20P, southwest Pacific), and Hurricane Igor (11L, North Atlantic).

these east-to-west propagating eddies are evident in the NCODA analyses (not shown).

5. Summary and discussion

In this study we investigated a number of questions about ocean responses to TCs by using six years of daily analyses of two measures of upper ocean energy content (i.e., OHC26C and T100M) in conjunction with the historical TC records. The investigation focused on composite analyses that show the type, magnitude, and persistence of upper ocean response to TC passage as a function of initial ocean conditions, latitude, translation speed, intensity, and KE and then discussed possible relationships between these factors and the upper ocean response.

Previous studies suggesting a ''local memory'' to TC passage with respect to SSTs and SST recovery times of approximately 30 days were reconfirmed. The 10-day lagged decrease of energy in the upper ocean was observed to be between about 5 and 20 kJ cm^{-2} based on median OHC26C. Ten days following TC passage, the temperature in the upper 100 m of the ocean also cooled between 0.3° and 0.7°C. We also found that variations in TC KE played a role in cooling the upper ocean, and that the size information in the TC best tracks (radii of 34-, 50-, and 64-kt winds) produces physically intuitive composite results and thus appears adequate for creating KE statistics like the ones used in this study.

Multiple linear regression parameterizations for estimating 5-, 10-, 20-, and 30-day changes in ocean heat content and SST based on routinely available data were also created using regression analysis and the composited data. These parameterizations suggest that SST cooling is best estimated as a function of latitude and our simplified KE (as defined in section 3). We also acknowledge that the latitude may be serving as a proxy for translation speed, which has been shown to be a predictor for cooling (Dare and McBride 2011), and that friction velocity, if it were available, would likely be better related to ocean mixing. In our composite SST, results that were stratified by translation speed were noisier than composites of OHC26C and T100M. The latitudinal dependence suggests that other conditions (subsurface ocean conditions, translation speed, and storm-induced Ekman processes) are likely also important for SST cooling and that those combined factors are well explained by latitude variation. On the other hand, cooling in the entire upper ocean is best parameterized as a function of KE, translation speed, and the initial upper ocean conditions, which is more physically enlightening.

According to these simple linear relationships, after 10 days a typical hurricane results in a 12 kJ cm^{-2} reduction of OHC26C, cools the upper 100 m of the ocean

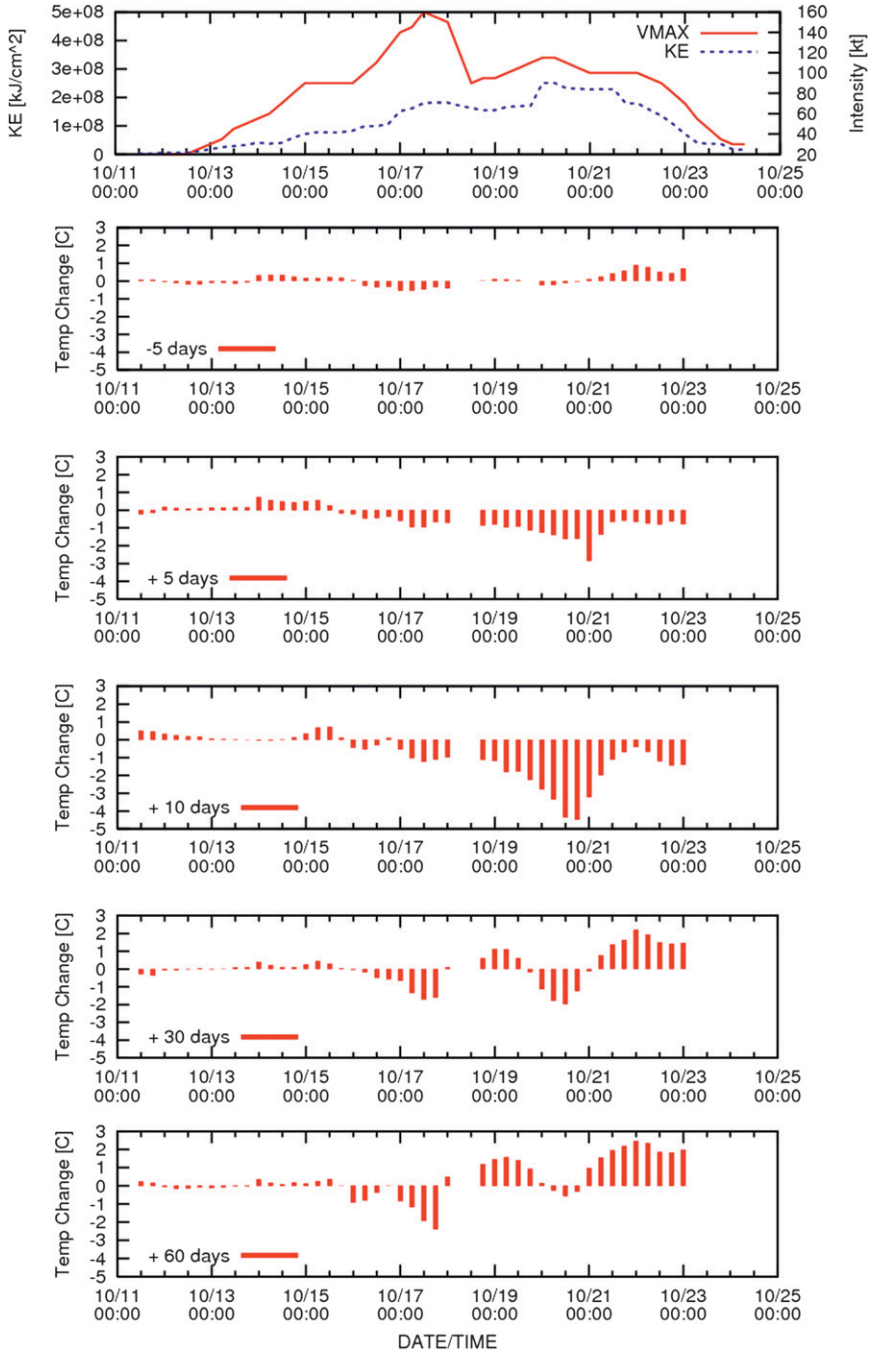

FIG. 10. Time series associated with Typhoon Megi (15W). Shown are the intensity and KE followed by the T100M changes observed 5 days prior to TC passage and 5, 10, 30, 60 days following TC passage. Dates and times valid at TC passage (i.e., lag 0).

0.5°C, and cools the local SST 0.7°C. Furthermore, a significant signal of SST cooling and reduction of upper ocean energy persists through 30 days. Thirty days after the typical TC passes similar regression equation predict a lingering 7 kJ cm^{-2} anomaly of OHC26C, a 0.7°C SST anomaly, and a 0.5°C T100M anomaly. It should be noted that the TC influence on the SST cooling decreases significantly from 20 to 30 days after TC passage, and latitude becomes more heavily weighted in the parameterization of SST. This result suggests that the TC's influence on SST changes does not extend much beyond 30 days and the 30-day SST parameterization should be used with

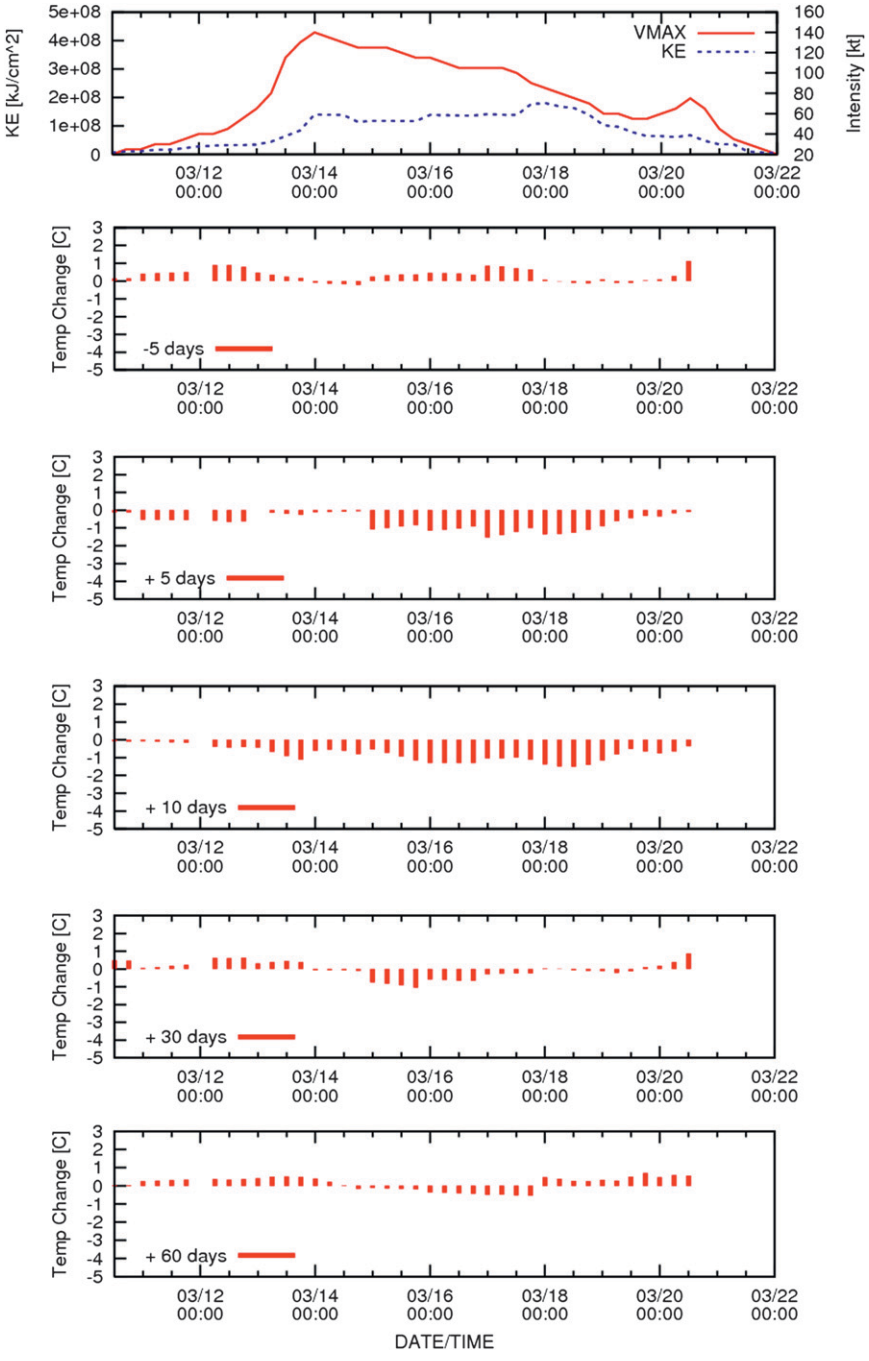

FIG. 11. As in Fig. 10, but for Tropical Cyclone Ului (20P).

caution—noting that the 20-day lagged SST cooling is 0.6°C. These simple estimates, however, allow for a simple energy budget to be constructed based on the number of storms, their tracks, and their sizes.

We also find that the depressed ocean heat content, much like lower SST, persists for at least 30 days and possibly as long as 60 days. Our results suggest that the ocean recovers slowly enough (means and medians do not recover fully in 90 days) that the interannual (e.g., ENSO) and interseasonal (e.g., winter) signals mask the TC effects. These results agree with the statements made in Jansen et al. (2010) that the upper ocean cold anomaly is on average not fully restored by surface fluxes before the mixed layer deepens in winter. This lack of recovery by the return of winter may be why latitude is so heavily weighted in our SST parameterizations and high-latitude

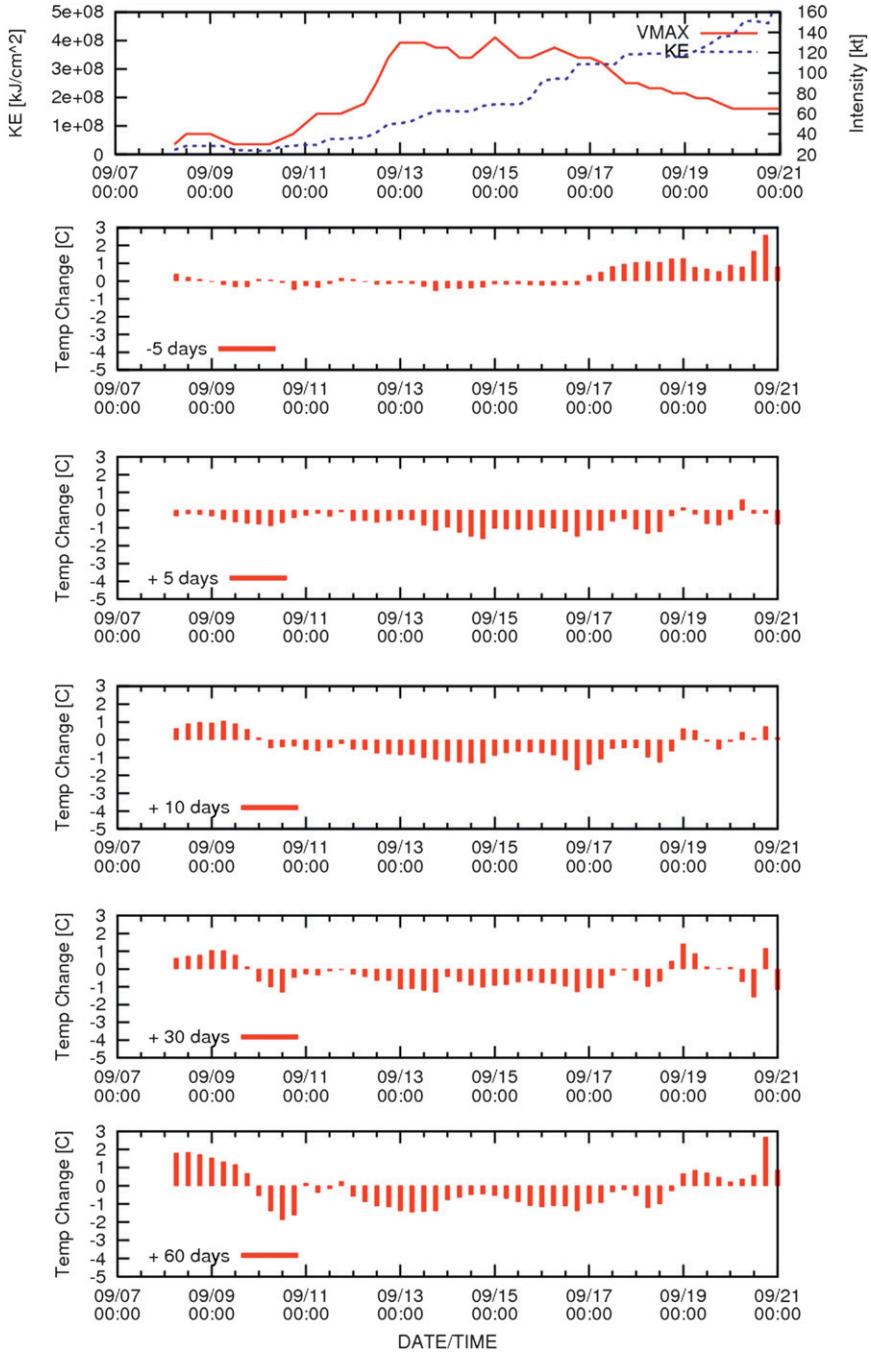

FIG. 12. As in Fig. 10, but for Hurricane Igor (11L).

cooling estimates appear too large, particularly at high latitudes and for the 30-day lagged SST cooling.

Furthermore, our findings suggest that there could be a negative feedback between the number and intensity of TCs and the ocean energy available for additional TCs that pass over recently TC-cooled ocean regions during a single TC season (i.e., 10 to 60 days). These findings reinforce the speculation of Landsea et al. (1998), who hypothesized that the pronounced intraseasonal variation of TCs in the Atlantic in 1995 (active August, inactive September, and active October) may have partially been due to oceanic cooling resulting from the hyperactive early TC season. However, a careful examination of the evidence is still needed to confirm their speculation.

In our examination of the T100M metric for ocean energy, we found evidence that the 100-m depth (used as a proxy for the mixed layer depth) may not be appropriate for basins where the thermocline is relatively shallow (e.g., eastern Pacific). This reinforces the findings of Shay and Brewster (2010), who showed that the greater stability of the east Pacific reduces the measurement of T100M to a fairly useless quantity with respect to TCs. Furthermore, this inference suggests that metrics that directly determine the average temperature in the mixed layer [e.g., the mixed layer definitions in Price (2009)] are more universally applicable to TC applications. Analyzing the oceanic mixed layer energy content, as indicated by temperature, stability, and density gradients is a subject of future work. The findings of this study, however, will also help guide future TC research and application development, especially with respect to potential intensity relationships used in TC forecast applications [e.g., operational models such as the Statistical Hurricane Intensity Prediction Scheme (SHIPS; DeMaria et al. 2005), the Statistical Typhoon Intensity Prediction Scheme (STIPS; Knaff et al. 2005), and the Logistic Grow Equation Model (LGEM; DeMaria 2009)].

Acknowledgments. The views, opinions, and findings contained in this report are those of the authors and should not be construed as an official National Oceanic and Atmospheric Administration or U.S. government position, policy, or decision. The authors thank Chris Landsea and the other two anonymous reviewers for their constructive comments and for ultimately improving the original manuscript. This work is funded by the Office of Naval Research and NOAA's Hurricane Forecast Improvement Program through the National Ocean Partnership Program.

REFERENCES

Black, P. G., 1983: Ocean temperature changes induced by tropical cyclones. Ph.D. dissertation, Pennsylvania State University, 278 pp.

——, and Coauthors, 2007: Air–sea exchange in hurricanes: Synthesis of observations from the Coupled Boundary Layer Air–Sea Transfer experiment. *Bull. Amer. Meteor. Soc.,* **88,** 357–384.

Cione, J. J., and E. W. Uhlhorn, 2003: Sea surface temperature variability in hurricanes: Implications with respect to intensity change. *Mon. Wea. Rev.,* **131,** 1783–1796.

Cummings, J. A., 2005: Operational multivariate ocean data assimilation. *Quart. J. Roy. Meteor. Soc.,* **131,** 3583–3604.

——, 2011: Ocean data quality control. *Operational Oceanography in the 21st Century,* A. Schiller and G. Brassington, Eds., Springer, 91–121.

Dare, R. A., and J. L. McBride, 2011: Sea surface temperature response to tropical cyclones. *Mon. Wea. Rev.,* **139,** 3798–3808.

D'Asaro, E. A., T. B. Sanford, P. Niiler, and E. Terrill, 2007: Cold wake of Hurricane Francis. *Geophys. Res. Lett.,* **34,** L15609, doi:10.1029/2007GL030160.

DeMaria, M., 2009: A simplified dynamical system for tropical cyclone intensity prediction. *Mon. Wea. Rev.,* **137,** 68–82.

——, and J. Kaplan, 1994: Sea surface temperature and the maximum intensity of Atlantic tropical cyclones. *J. Climate,* **7,** 1324–1334.

——, M. Mainelli, L. K. Shay, J. A. Knaff, and J. Kaplan, 2005: Further improvements to the Statistical Hurricane Intensity Prediction Scheme (SHIPS). *Wea. Forecasting,* **20,** 531–543.

Demuth, J., M. DeMaria, and J. A. Knaff, 2006: Improvement of Advanced Microwave Sounding Unit tropical cyclone intensity and size estimation algorithms. *J. Appl. Meteor. Climatol.,* **45,** 1573–1581.

Emanuel, K. A., 1986: An air–sea interaction theory for tropical cyclones. Part I: Steady-state maintenance. *J. Atmos. Sci.,* **43,** 585–605.

——, 1991: The theory of hurricanes. *Annu. Rev. Fluid Mech.,* **23,** 179–196.

Fox, D. N., W. J. Teague, C. N. Barron, M. R. Carnes, and C. M. Lee, 2002: The Modular Ocean Data Assimilation System (MODAS). *J. Atmos. Oceanic Technol.,* **19,** 240–252.

Frank, W. M., 1977: The structure and energetics of the tropical cyclone I. Storm structure. *Mon. Wea. Rev.,* **105,** 1119–1135.

Goni, G., and Coauthors, 2009: Applications of satellite-derived ocean measurements to tropical cyclone intensity forecasting. *Oceanography,* **22,** 190–197.

Gray, W. M., 1979: Hurricanes: Their formation, structure and likely role in the tropical circulation. *Meteorology over the Tropical Oceans,* D. B. Shaw, Ed., Royal Meteorological Society, 155–218.

Hart, R. E., R. N. Maue, and M. C. Watson, 2007: Estimating local memory of tropical cyclones through MPI anomaly evolution. *Mon. Wea. Rev.,* **135,** 3990–4005.

Holland, G. J., 1997: The maximum potential intensity of tropical cyclones. *J. Atmos. Sci.,* **54,** 2519–2541.

Holliday, C. R., and A. H. Thompson, 1979: Climatological characteristics of rapidly intensifying typhoons. *Mon. Wea. Rev.,* **107,** 1022–1034.

Jacob, S. D., L. K. Shay, A. J. Mariano, and P. G. Black, 2000: The 3D oceanic mixed layer response to Hurricane Gilbert. *J. Phys. Oceanogr.,* **30,** 1407–1429.

Jansen, M. F., R. Ferrari, and T. A. Mooring, 2010: Seasonal versus permanent thermocline warming by tropical cyclones. *Geophys. Res. Lett.,* **37,** L03602, doi:10.1029/2009GL041808.

Knaff, J. A., and C. R. Sampson, 2009: Southern Hemisphere tropical cyclone intensity forecast methods used at the Joint Typhoon Warning Center. Part II: Statistical–dynamical forecasts. *Aust. Meteor. Oceanogr. J.,* **58,** 9–18.

——, ——, and M. DeMaria, 2005: An operational statistical typhoon intensity prediction scheme for the western North Pacific. *Wea. Forecasting,* **20,** 688–699.

——, ——, ——, T. P. Marchok, J. M. Gross, and C. J. McAdie, 2007: Statistical tropical cyclone wind radii prediction using climatology and persistence. *Wea. Forecasting,* **22,** 781–791.

Kraus, E. B., and J. Turner, 1967: A one-dimensional model of the seasonal thermocline. II. The general theory and its consequences. *Tellus,* **19,** 98–106.

Landis, R. C., and D. F. Leipper, 1968: Effects of Hurricane Betsy upon Atlantic Ocean temperature, based upon radio-transmitted data. *J. Appl. Meteor.,* **7,** 554–562.

Landsea, C. W., G. D. Bell, W. M. Gray, and S. B. Goldenberg, 1998: The extremely active 1995 Atlantic hurricane season: Environmental conditions and verification of seasonal forecasts *Mon. Wea. Rev.,* **126,** 1174–1193.

——, B. A. Harper, K. Hoarau, and J. A. Knaff, 2006: Can we detect trends in extreme tropical cyclones? *Science,* **313,** 452–454.

Leipper, D., and D. Volgenau, 1972: Hurricane heat content of the Gulf of Mexico. *J. Phys. Oceanogr.,* **2,** 218–224.

Lin, I.-I., C.-C. Wu, I.-F. Pun, and D.-S. Ko, 2008: Upper-ocean thermal structure and the western North Pacific category 5 typhoons. Part I: Ocean features and the category 5 typhoons' intensification. *Mon. Wea. Rev.,* **136,** 3288–3306.

——, I.-F. Pun, and C.-C. Wu, 2009: Upper-ocean thermal structure and the western North Pacific category 5 typhoons. Part II: Dependence on translation speed. *Mon. Wea. Rev.,* **137,** 3744–3757.

Maclay, K. S., M. DeMaria, and T. H. Vonder Haar, 2008: Tropical cyclone inner-core kinetic energy evolution. *Mon. Wea. Rev.,* **136,** 4882–4898.

Merrill, R. T., 1984: A comparison of large and small tropical cyclones. *Mon. Wea. Rev.,* **112,** 1408–1418.

——, 1987: An experiment in statistical prediction of tropical cyclone intensity change. NOAA Tech Memo. NWS NHC-34, 34 pp.

Miller, B. I., 1958: On the maximum intensity of hurricanes. *J. Meteor.,* **15,** 184–195.

Palmén, E., 1948: On the formation and structure of tropical cyclones. *Geophyisica,* **3,** 26–38.

Perlroth, I., 1967: Hurricane behavior as related to oceanographic environmental conditions. *Tellus,* **19,** 258–268.

Phillips, O. M., 1977: *The Dynamics of the Upper Ocean.* 2nd ed. Cambridge University Press, 336 pp.

Pollard, R. T., P. B. Rhines, and R. O. R. Y. Thompson, 1973: The deepening of the wind-mixed layer. *Geophys. Fluid Dyn.,* **3,** 381–404.

Price, J. F., 1981: Upper ocean response to a hurricane. *J. Phys. Oceanogr.,* **11,** 153–175.

——, 2009: Metrics of hurricane–ocean interaction: Vertically-integrated or vertically-averaged ocean temperature? *Ocean Sci.,* **5,** 351–368.

Riehl, H., 1950: A model for hurricane formation. *J. Appl. Phys.,* **21,** 917–925.

Sampson, C. R., and A. J. Schrader, 2000: The automated tropical cyclone forecasting system (version 3.2). *Bull. Amer. Meteor. Soc.,* **81,** 1231–1240.

Sanford, T. B., J. F. Price, J. Girton, and D. C. Webb, 2007: Highly resolved observations and simulations of the ocean response to a hurricane. *Geophys. Res. Lett.,* **34,** L13604, doi:10.1029/2007GL029679.

Schwerdt, R. W., F. P. Ho, and R. R. Watkins, 1979: Meteorological criteria for standard project hurricane and probable maximum hurricane wind fields, Gulf and East Coasts of the United States. NOAA Tech. Rep. NWS 23, 317 pp.

Shay, L. K., and E. W. Uhlhorn, 2008: Loop current response to Hurricanes Isidore and Lili. *Mon. Wea. Rev.,* **136,** 3248–3274.

——, and J. K. Brewster, 2010: Oceanic heat content variability in the eastern Pacific Ocean for hurricane intensity forecasting. *Mon. Wea. Rev.,* **138,** 2110–2131.

——, P. G. Black, A. J. Mariano, J. D. Hawkins, and R. L. Elsberry, 1992: Upper ocean response to Hurricane Gilbert. *J. Geophys. Res.,* **97,** 20 227–20 248.

——, A. J. Mariano, S. D. Jacob, and E. H. Rayan, 1998: Mean and near-inertial ocean current response to Hurricane Gilbert. *J. Phys. Oceanogr.,* **28,** 858–889.

——, G. J. Goni, and P. G. Black, 2000: Effects of a warm oceanic feature on Hurricane Opal. *Mon. Wea. Rev.,* **128,** 1366–1383.

Uhlhorn, E., and L. K. Shay, 2012: Loop Current mixed layer energy response to Hurricane Lili (2002). Part I: Observations. *J. Phys. Oceanogr.,* **42,** 400–419.

Whitney, L. D., and J. S. Hobgood, 1997: The relationship between sea surface temperatures and maximum intensities of tropical cyclones in the eastern North Pacific Ocean. *J. Climate,* **10,** 2921–2930.